In situ deposition of M(M=Zn; Ni; Co)-MOF-74 over structured carriers for cyclohexene oxidation - Spectroscopic and microscopic characterisation

P.J. Jodłowski [a],[**], G. Kurowski [a], K. Dymek [a], R.J. Jędrzejczyk [b], P. Jeleń [c], Ł. Kuterasiński [d], A. Gancarczyk [e], A. Węgrzynowicz [a], T. Sawoszczuk [f], M. Sitarz [c]

[a] *Faculty of Chemical Engineering and Technology, Cracow University of Technology, Warszawska 24, 30-155, Kraków, Poland*
[b] *Malopolska Centre of Biotechnology, Gronostajowa 7A, 30-387, Kraków, Poland*
[c] *Faculty of Materials Science and Ceramics, AGH University of Science and Technology, Mickiewicza 30, 30-059, Kraków, Poland*
[d] *Jerzy Haber Institute of Catalysis and Surface Chemistry, Polish Academy of Sciences, Niezapominajek 8, 30-239, Kraków, Poland*
[e] *Institute of Chemical Engineering, Polish Academy of Sciences, Bałtycka 5, 44-100, Gliwice, Poland*
[f] *Institute of Quality Sciences and Product Management, Cracow University of Economics, Rakowicka 27, 31 - 510, Kraków, Poland*

A B S T R A C T

The aim of this study was to obtain and characterise thin metal organic frameworks layers supported on various metallic structured carriers such as FeCrAl plates and woven gauzes and NiCr foams. The thin layers of the metal organic frameworks were fabricated by *in situ* solvothermal deposition, optimised by the selection of metal precursor and the layering/washing order. The parameters of the resulting metal organic framework coatings were characterised in terms of layer thickness in correlation with the fold overlap, morphology, chemical properties and mechanical resistance to ultrasonic irradiation. Several techniques were used to characterise metal-organic framework layers, including *in situ* FTIR, μRaman mapping, XRD, low temperature sorption of liquid nitrogen, and SEM. The results of structural analysis of prepared structured catalysts revealed that the surfaces of the structured carriers are uniformly covered with Me-MOF-74 thin layers. The mechanical stability tests showed that the metallic foams possessed high mechanical resistance and may be considered as a structured support for heterogeneous catalysts.

1. Introduction

Metal-organic framework, denoted as MOF, is defined by the International Union of Pure and Applied Chemistry (IUPAC) as "*a coordination network with organic ligands containing potential voids*" [1]. Since the early 1990s, after the first scientific reports on the development of a new class of porous materials, there has been strong interest in this topic. Almost 30 years of intense research has led to numerous potential applications of MOFs in a wide variety of fields including gas adsorption, separation, catalysis, photocatalysis and bio-sensing. Intensive studies on MOF applications have also included their application in fuel cells and supercapacitors [2–9]. Several synthesis routes of metal-organic networks have been developed over the years. The most utilised are conventional solvothermal and non-solvothermal, microwave-assisted and mechanochemical methods [2,4,10]. Numerous scientific papers report on both solvothermal and non-solvothermal syntheses of MOFs, giving the exact synthesis procedures, and the changes of MOFs'

parameters by the modification of synthesis conditions can be found in the literature. Several MOFs have been synthesised using non-solvothermal methods which require the selection of metal precursors, organic linkers and solvents, as well as the appropriate synthesis temperature. The remarkable success of MOFs in a wide range of applications has pushed scientists to use MOF materials as precursors to obtain catalytic materials with unprecedented properties. However, despite the fact that the recent development in synthesis of metal organic frameworks pushes the limits of the chemical and mechanical resistance of those materials, they are used in a wide range of industrial applications based on catalysis. The next milestone in the application of metal organic frameworks in industry may be not only further improvements in the chemical and mechanical endurance of those materials, but also their structuring into monolith-like, short channel structures membranes or arranged structures which guarantees high heat and mass transport properties. Since the remarkable success in development of structured catalysts in industry-based heterogeneous

---

catalysts including gas exhaust abatement in the automotive sector and stationary source abatement, water gas shift, combustion and NOx abatement [11], the structuring of MOFs into structured catalysts seems to be a natural step forward in their evolution.

Several works have recently been published describing the ways of the preparation of structured materials based on metal organic frameworks [12–18]. In the work written by Chen et al. [18], various attempts to produce composite HKUST/Fe$_3$O$_4$ materials in different bodies like pellets, films and foams are described. The authors have developed a method of shaping of composite HKUST/Fe$_3$O$_4$ materials by using carboxymethylcellulose as a binder. By using freeze-drying or gel-induced surface hardening, various foam-like or thin films with high porosity properties have been developed. A complementary method for the preparation of MOF-based foams is described in the work published by Garai et al. [19], where the shaping of metal organic frameworks by transferring them into areogel or xerogel and further solvent removal was proposed. However, despite the versatility of proposed method, the use of foams derived by the aerogel and xerogel method is limited, due to a high fragility of derived structures. In the deposition of metal organic frameworks on the metallic surfaces, much attention has been paid to the preparation of electrodes for lithium-ion batteries [20]. The deposition of metal organic frameworks based on zeolite-imidazole frameworks was performed by annealing treatment. The porous zinc-cobalt oxide porous plates prepared in this way revealed remarkable, high reversible properties as anode materials and considerable lithium storage capacities.

Despite the fact that the metal organic framework materials demonstrate great catalytic properties in many catalytic reactions including catalytic oxidation [21–25], selective catalytic reduction [26], alkylation, transesterification [10], water gas shift and conversion of methane to fuels, their heat and mass transfer properties may be successfully tuned up by either their direct shaping into structured catalysts or their deposition on existing carriers. Although several works describing the use of three-dimensional printing of metal organic frameworks to monoliths have recently been published [17], literature reports describing deposition of MOFs on supported carriers are scarce.

Structural reactors owe their significant success mainly to their wide use in the automotive and energy industries, where the ceramic or metal monoliths are commonly in use for oxidation and selective catalytic reduction reactions [27]. The catalytic oxidation of hydrocarbons is one of the most important reactions for the conversion of hydrocarbons to obtain valuable products. Over the numerous catalytic reactions, the oxidation of cyclic hydrocarbons such as cyclohexane or cyclohexene results in the formation of value-added products that can be further used in fine chemical synthesis. The exemplary oxidation of cyclohexene with H$_2$O$_2$ may be used as an alternative method for the synthesis of adipic acid, which is further used in production of Nylon-66 [23]. Additionally, the oxidation of cyclohexene may also result in the formation of epoxides and unsaturated ketones and alcohols which are valuable products in organic syntheses and the fragrance industry. Recently, the catalytic oxidation of cyclohexenene to the mixture of oxygen-containing products has been reported for SBA-15 [28], core shell-structures [24] and MIL-101 [21] or modified Ni-MOF-74 catalyst [29]. Although literature reports provide information on the successful use of metal organic frameworks on cyclohexene catalytic oxidation instead of conventional mesoporous catalysts, a common feature of the work is the use of powder catalysts which practically eliminates their wider application. The main reason for that is the necessity of additional mixture/catalyst filtration to receive products instead of simple structured catalyst removal from the batch reactor.

In this work, we present an optimised method for the preparation of composite metal organic frameworks for structured catalysts based on metallic plates, woven gauzes and metallic foams as catalysts for aerobic oxidation of cyclohexene. The choice of those types of structures is not accidental, as they are used as catalyst supports: metal monoliths for oxidation and reduction reactions, meshes for oxidation/separation

processes and foams for oxidation reactions. The prepared structured catalysts with deposited thin metal organic frameworks have revealed considerable surface areas and remarkable, good adhesion parameters. The catalytic activity tests have proven that the composite metal organic framework catalysts may be successfully used in aerobic oxidation of cyclohexene to produce value-added fine chemicals.

2. Experimental

All chemicals used in this study were reagent grade and are commercially available. They include nickel acetate tetrahydrate, cobalt acetate tetrahydrate, zinc acetate dihydrate, nickel nitrate hexahydrate, cobalt nitrate hexahydrate, zinc nitrate hexahydrate, 2,5-dihydroxyterephthalic acid (DHTP), all from Sigma-Aldrich, and methylene chloride, n-hexane, N,N-dimethylformamide (DMF), n-propanol, from Chempur Poland.

2.1. Synthesis

The synthesis protocol used in this study consisted of three steps: support pre-treatment, *in situ* MOF deposition and material activation. Structured supports used in this study were FeCrAl plate (GoodFellow, 0.3 mm thick Fe 72.8%, Cr 22%, Al 5%, Y 0.1%, Zr 0.1%), steel woven gauzes (17.5 mesh/in., wire diameter 0.1 mm; Fe 73%, Cr 20%, Al 5%) and NiCr foams (Recemat BV; 27–33 ppi, estimated average pore diameter 0.6 mm, Ni 60–80%, Cr 15–40%, Fe 0.5%, Cu 0.1–0.3%).

Prior to the deposition of MOF on to the structured carriers, the structures were cut into small pieces – FeCrAl plates 1 cm × 1 cm, FeCrAl gauze 1 cm × 1 cm, NiCr foams 1 cm × 1 cm – and subsequently cleaned in an ultrasound bath using acetone, n-propanol and distilled water to remove impurities. Subsequently, FeCrAl plates and wire gauzes were calcined at 1100 °C in a ventilated oven for 24 h to obtain a thin alumina layer. This procedure of FeCrAl alloy treatment was previously reported as enhancing further adhesion between alloy and deposited material [30].

In the second step, the M(M = Zn; Ni; Co)–MOF-74 layers were deposited *in situ* by modifying the solvothermal method for powder synthesis recently reported in the literature [31,32]. The detailed synthesis conditions are summarised in Table 1.

2.1.1. Synthesis of Zn-MOF-74 layers

The first layer deposition of Zn-MOF-74 was performed from Solution I by using zinc acetate as a metal precursor. After dissolution of the appropriate amounts (see Table 1) of metal salt and 2,5-dihydroxyterephtalic acid (DHTP) in N,N-dimethylformamide DMF, the metal salt solution was added to the DHTP solution dropwise to avoid precipitation. The resulting solution was then transferred to Teflon liners with structured carriers previously suspended on scaffolding. The as prepared stainless-steel bombs with Teflon vessels were tightly capped and placed in oven at 100 °C for 20 h. The resulting structured carriers with deposited MOF layers and non-deposited MOF crystals were washed using the sequence proposed elsewhere [33]: methyl chloride three times, and n-hexane three times. The resulting materials were then dried at room temperature and activated in a vacuum drier at 180 °C for 6 h. The double and triple deposition of Zn-MOF-74 was performed by changing synthesis solution I to synthesis solution II with zinc nitrate as a metal precursor.

2.1.2. Synthesis of Co-MOF-74 and Ni-MOF-74 layers

The general procedure for deposition of Co-MOF-74 and Ni-MOF-74 was performed as for deposition of Zn-MOF-74, with the difference that the appropriate metal nitrate (Co or Ni) was used as a metal precursor in all three-layer deposition steps.

Table 1
Detailed synthesis conditions and colour measurement results.

Me-MOF-74 (Me: Zn, Ni, Co)	Synthesis solution I	Synthesis solution II	Synthesis temperature, [°C]	Synthesis time, [h]	Measured colour, HEX	Measured colour, RGB
Zn-MOF-74	0.75 mmol (2.5DHTP) 2.3 mmol $Zn(CH_3COO)_2 \cdot 2H_2O$ 30 ml DMF, 1.5 ml H_2O	0.75 mmol (2.5DHTP) 2.3 mmol $Zn(NO_3)_2 \cdot 6H_2O$ 30 ml DMF, 1.5 ml H_2O	100	20	#F8E8A3	248;232;163
Ni-MOF-74	-	0.75 mmol (2.5DHTP) 2.6 mmol $Ni(NO_3)_2 \cdot 6H_2O$ 30 ml DMF, 1.5 ml H_2O			#DCAA3B	220;170;59
Co-MOF-74	-	0.75 mmol (2.5DHTP) 2.6 mmol $Co(NO_3)_2 \cdot 6H_2O$ 30 ml DMF, 1.5 ml H_2O			#A26940	162;105;64

2.2. Characterisation

The crystallinity of prepared materials was determined by XRD analyses using an X'Pert Pro MPD (PANalytical) diffractometer with CuK$_\alpha$ radiation at 30 mA and 40 kV. The diffraction patterns were collected in the range of 5–80° 2θ with a 0.033° step for 12 min. The determination of crystallinity M(M = Zn; Ni; Co)-MOF-74 layers deposited on FeCrAl plates was determined by means of Grazing Incidence X-Ray Diffraction analysis (GIXRD). Analyses were performed only for M(M = Zn; Ni; Co)-MOF-74 layers deposited on FeCrAl plates due to the GIXRD method limitations. The GIXRD analyses were performed in 5–75° 2θ range with a 0.033° and constant omega angle 1°.

The morphology of prepared structured catalysts was determined by using a Nova Nano SEM 300 FEI Company scanning electron microscope for high-quality magnification imaging. To enhance the visibility of the structure of and the distribution of the Me-MOF-74 layers on structured carriers, the obtained materials were pseudo-coloured using Fiji software. The exact colours of LUT's were determined of an activated MOF samples by using AvaSpec-ULS3648 High-resolution spectrometer equipped with a high-temperature reflection probe (FCR-7UV400-2-ME-HTX, 7 × 400 μm fibres, Avantes BV) and a Mikropack DH-2000-BAL Deuterium-Tungsten Halogen Light Source working in the 200–1000 nm spectral range. The exact colour of the prepared material was determined by AvaSoft 8 software with colour measurements extension (Avantes BV). The determined colours were presented using HEX and RGB values (Table 1).

Kr and N_2 sorption experiments were performed on ASAP 2020 (Micromeritics) for structured supports, powder samples and MOF layers deposited on FeCr plates and NiCr foams, respectively. Prior to analyses, the samples were outgassed at 250 °C for 12 h. The BET specific surface areas were calculated for p/p$_0$ in the range of 0.06–0.2 and for Kr adsorption and p/p$_0$ = 0.06–0.2 for N_2 adsorption experiments.

The Me-MOF-74 layers deposited on FeCrAl plates were examined by X-ray Photoelectron Spectroscopy with an ESCA Prevac spectrometer equipped with a hemispheric XPS analyser of charged particles and AES analysers (VG Scienta R3000) and Mg/Al anticathodes. The sample charging effect was corrected using C 1s band at 248.8 eV.

The prepared Me-MOF-74 samples were characterised by FTIR spectroscopy using two modes: ATR FTIR for non-deposited MOF crystals that were collected after *in situ* MOF deposition, and by *in situ* DRIFT for composite Me-MOF-74 samples deposited on FeCrAl plates. The ATR-FTIR studies were carried out using a Bruker Vertex 70v spectrometer equipped with Bruker Platinum ATR (diamond crystal), by averaging 128 scans in the range of 4000–400 cm^{-1} with a 4 cm^{-1} resolution. The *in situ* DRIFT spectra were collected by using a Thermo Nicolet iS 10 equipped with MCT detector and Praying Mantis High Temperature Reaction Chamber with ZnSe windows (Harrick). The *in situ* experiments were performed on dehydrated at 110 °C for 1 h in He flow (AirProducts) catalysts samples. To avoid the presence of water and oxygen, the He line was equipped with an Agilent moisture/oxygen trap. The spectra were collected by averaging 128 scans with 4 cm^{-1} resolution and BaSO$_4$ as a background.

The FTIR sorption experiments by using CO (Linde) and CD$_3$CN as probe molecules were performed by using a NICOLET iS 10 spectrometer. The spectra were taken in the 4000-650 cm^{-1} range with 4 cm^{-1} resolution by averaging 128 scans. Prior to the spectroscopic measurements, the obtained Me-MOF-74 crystals were pressed into the self-supporting wafers and activated under vacuum at 270 °C with 5 °C/min temperature ramp. The qualitative determination of the nature of the active sites in prepared MOF-74 samples was determined by low temperature (-100 °C) carbon monoxide (Linde) and room temperature CD$_3$CN (Sigma Aldrich) chemisorption. Prior to the chemisorption of probe molecules, the adsorbed gases were distilled by freeze and thaw cycles to remove impurities. The resulting spectra were presented as a substructured spectra after each portion of adsorbed probe molecule and activated sample as a background.

To determine the nature and the chemical distribution of deposited metal organic frameworks on structured carriers, the μRaman mapping analyses were performed by using high resolution confocal Raman microscope - Witec Alpha 300 M+ equipped with three ZEISS lenses (x10, x50, x100), two diffraction gratings 600 and 1800, and two 633 nm and 488 nm with power of approximately 50 and 75 mW, respectively. The μRaman spectra were taken for FeCrAl plates due to the optical microscope limitations.

The effectiveness and stability of the prepared structured metal organic framework materials was determined in two ways. The effectiveness of MOF-74 *in situ* deposition was determined by weighing the washed and activated composite materials before and after layering. The mechanical stability test was performed by ultrasound irradiation methods proposed recently in literature for structured catalysts [34–36]. In brief, the washed and activated structured catalysts were immersed in polypropylene jars filled with n-propanol and irradiated in a 40 kHz ultrasound bath (Ultrasonix proclean 0.7 M, 60 W). The weight loss was determined after 15 min of ultrasonic irradiation.

2.3. Catalytic activity

Catalytic activity during the aerobic oxidation of cyclohexene was measured under atmospheric and 10 bar O$_2$ pressure for powder samples and MOF deposited on NiCr foams as representative for structured catalysts. The aerobic oxidation of cyclohexene was measured under atmospheric conditions and were performed in glass reactor vessel equipped with a reflux condenser. In a typical experiment, the 50 mg of catalyst (for MOF/NiCr foams 50 mg of catalyst refers to the 50 mg of MOF deposited on NiCr foam) and 10 cm^3 of cyclohexene were placed in the reactor and heated to 80 °C for 4 h under oxygen flow. The oxygen flow (Oxygen 5.0, Linde Gas) was controlled by Bronkhorst mass flow-meters and set to 20 ml/min. Prior to the reaction, the glass reactor was

purged with molecular oxygen for 15 min with 20 ml/min flow. The experiments under 10 bar O$_2$ pressure were performed in a Buchi Mini-clave Stainless Steel reactor. The catalytic experiment procedure was similar to experiments at atmospheric pressure. The O$_2$ pressure was set to 10 bar by using a Buchi manometer at the reactor vessel. Prior to the catalytic experiments, the pressure reactor was purged with molecular oxygen for 15 min.

The catalytic reaction products were analysed by the method described in ref. [21], using a gas chromatograph (Thermo Scientific A Trace 1310) coupled with a single quadrupole mass spectrometer (ISQ) equipped with an RXi-5MS capillary column (Restek, USA, 30 m, 0.25 mm ID, 0.25 mm film thickness.). Prior to analysis, the reacting mixtures were thoroughly cooled down in an ice bath to avoid CH evaporation, and approx. 10 mg of PPh$_3$ was added to reduce cyclohexenyl hydro-peroxide to 2-cyclohexen-1-ol and avoid further mixture oxidation.

The migration of metal (Zn, Ni, Co) from prepared MOF samples to the reaction mixture during the catalytic reaction was determined by atomic absorption spectrometry using a Thermo Scientific ICE3000 series AAS spectrometer (Thermo Fisher Scientific, Waltham, MA, USA). To determine the metal content in post-reaction mixtures, the external standard method was used. The results were processed using Solaar 2.01 software. All standards and reagents were of trace analysis grade.

3. Results and discussion

The synthesis of metal organic frameworks may be performed in various conditions by using metal precursors and organic linkers, of which metal nitrates and acetates are commonly used [2]. Since the choice of the starting reagents for synthesis of MOF in powder form may influence the crystal size and the synthesis time, the application of the *in situ* crystal deposition over the metallic structures should consider crystal-surface interactions [37]. It followed from this that acetates and nitrates were natural choices due to their acidic properties in a liquid solution. The choice of the acetates and nitrates is dictated by their dual role as metal precursors and acidic environment generators. The acidic environment is favourable and commonly used in structured reactor preparation in metallic support pre-treatment [30]. It was previously reported that the use of an acidic environment induces the formation of thin alumina layer on FeCrAlloy material, which increases further adhesion of the deposited layer [38]. Another problem related to the nature of the precursor is that, while acetates can be used for synthesis of various MOF, their use for MOF-74 synthesis is limited for the preparation of Zn-MOF-74 though conventional synthesis and Ni- and Co-MOF-74 through dry-gel synthesis [39]. Based on available literature reports, we used zinc acetate as a starting point mixture in the optimisation of *in situ* synthesis. To monitor the acidity of the synthesis solutions, we performed measurements of pH before and after *in situ* solvothermal synthesis (Table 2). The acetate solutions' pH values before the synthesis are very close to neutral point, whereas

Table 2

pH values for different synthesis methods.

Me-MOF-74 (Me: Zn, Ni, Co)	pH			
	Metal acetate, Solution I		Metal nitrate precursor, Solution II	
	Prior solvothermal synthesis	After solvothermal synthesis	Prior solvothermal synthesis	After solvothermal synthesis
Zn-MOF-74	6.92 ± 0.07	8.78 ± 0.09	2.63 ± 0.03	6.87 ± 0.07
Ni-MOF-74	–	–	2.73 ± 0.03	6.39 ± 0.06
Co-MOF-74	–	–	2.72 ± 0.03	6.67 ± 0.07

nitrate-based precursor solutions are strongly acidic (pH ≈ 2.7). Despite the fact that the *in situ* synthesis of Zn-MOF-74 resulted in well crystallised MOF-74, as already been postulated in the literature [39,40], the amount of MOF-74 deposited on structured carriers was considerably low. Hence, for the double and triple synthesis of MOF layers on metallic supports, we used metal-nitrates as metal precursors. However, it has to be pointed out that the use of the metal nitrate as an MOF metal precursor at the first layer deposition did not result in either deposition of the MOF layer at the metallic carrier or formation of the Zn-MOF-74 crystals on the bottom of the reaction vessel. To confirm the crystallinity and the purity of obtained materials, PXRD for non-deposited powder MOF-74 (Fig. 1, left column) and GIXRD for MOF-74 deposited on FeCrAl plates (Fig. 1, right column) were performed. In all prepared materials, as well as for the non-deposited crystal phase and thin layer deposited on metallic carriers, the presence of Zn-MOF-74 (JCPDS 00-062-1198), Ni-MOF-74 (JCPDS 00-62-1029) and Co-MOF-74 (JCPDS 00-063-1147) structures without impurities [39,41,42] was confirmed. The use of GIXRD analysis allowed high quality diffraction patterns on MOF layers deposited on FeCrAl plates to be obtained. Despite the fact that the GIXRD measurement was performed at a low angle, we could still observe reflections at 25.6, 35.1, 37.8, 43.5, 52.6 (024) and 57.6°, which are characteristic of α-Al$_2$O$_3$ [43] (JCPD 04-005-4503) from FeCrAl support. The α-Al$_2$O$_3$ is the result of the FeCrAl support calcination at 1100 °C which enhances the adhesion of deposited MOF layers. The detailed phase analysis was previously reported in our previous paper [44] and also in GIXRD profile analysis in supporting information (Figs. S1-S2). It may be seen that the intensity of characteristic α-Al$_2$O$_3$ reflections decreases in the Co-MOF-74 >Ni-MOF-74> Zn-MOF-74 order, which may suggest that the thickness of metal organic framework layers in prepared structured catalysts increases. It is also worth mentioning that, in all considered materials, we observed that the crystallisation of MOF material over the metallic support was strongly influenced by the number of metallic supports placed in the Teflon liners for *in situ* deposition. Once the total amount of metallic supports exceeded 1 g per synthesis, we did not observe the metal organic

framework crystals either in reacting vessels or deposited on the structured carriers.

To determine the structure and the purity of the MOF layers deposited on FeCrAl plates, the XPS analysis of triple deposited MOF-74 layers on FeCrAl plates was performed. The results of the XPS analyses are presented in Fig. 2. The survey spectra of the triple deposited MOF-74 layers deposited on FeCrAl plates (black lines) and calcined FeCrAl plates are presented in Fig. 2 A, D, G. It may be seen that the survey spectra of Zn-MOF-74, Ni-MOF-74 and Co-MOF-74 do not reveal any lines originating from calcined FeCrAl plates (cf. red lines) and only signals from Me(Zn, Ni, Co) 2p, O1s and C1s may be observed. Since the alumina is mainly present at the calcined FeCrAl plate surface due to the migration of alumina at 1100 °C calcination, we used the signal at 75 eV originating from Al 2p [45] as an internal marker to determine the purity deposited MOF-74 layers. The zoomed area for 75 eV region for Me (Zn, Ni, Co)-MOF-74 catalysts are presented in Fig. 2 B, E, H. It may be seen that, for all considered cases, the Al 2p line does not occur at the XPS spectra of Me (Zn, Ni, Co)-MOF-74 catalysts. The XPS spectra for Zn 2p, Ni 2p and Co 2p for Me (Zn, Ni, Co)-MOF-74 are presented in Fig. 2 C, F, I. The Zn-MOF-74/FeCrAl catalyst reveal two main peaks at 1022.2 and 1045.3 eV (Fig. 2 C) that may be attributed to Zn 2p$_{3/2}$ and Zn 2p$_{1/2}$ [46]. For the Ni-MOF-74/FeCrAl catalyst two main group bands were detected with the peaks at 855.9 and 873.6 eV and associating satellite peaks at 860.7 and 879.4 eV, which may be attributed to Ni 2p$_{3/2}$ and Ni 2p$_{1/2}$ [47], respectively. At the XPS spectrum of Co-MOF-74/FeCrAl, catalyst peaks at 781.9 and 797.8 eV and associating satellite peaks at 785.8 and 802.6 eV are observed. These may be attributed to Co 2p$_{3/2}$ and Co 2p$_{1/2}$ [48], respectively.

The effectiveness of the *in situ* MOF deposition over structured supports was determined gravimetrically after each deposition. The results are presented in Fig. 3 A. The effectiveness of the MOF deposition on the structured carriers was presented as a mass increase per geometrical surface area of metallic support. Such deposition results are commonly used for the comparison of coating loading in structured reactors engineering [27,49]. The lowest MOF loading was observed for the layers
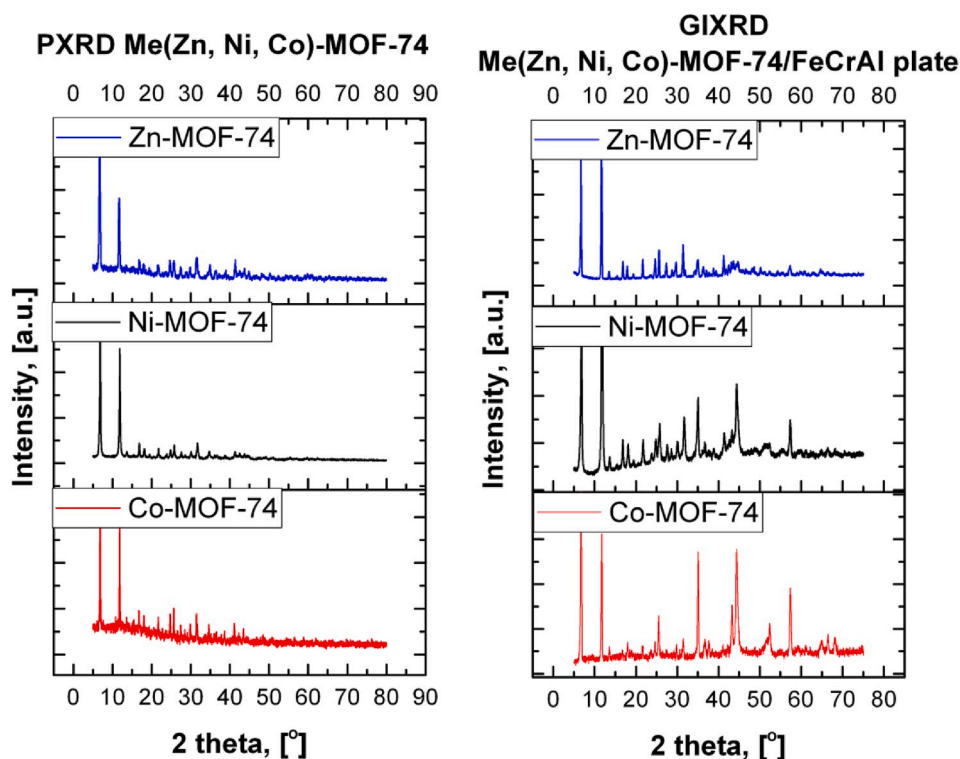

Fig. 1. XRD analysis of prepared materials; Left column: M(M = Zn; Ni; Co)-MOF-74 powders; right column: GIXRD of M(M = Zn; Ni; Co)-MOF-74 triple deposited FeCrAl supports.
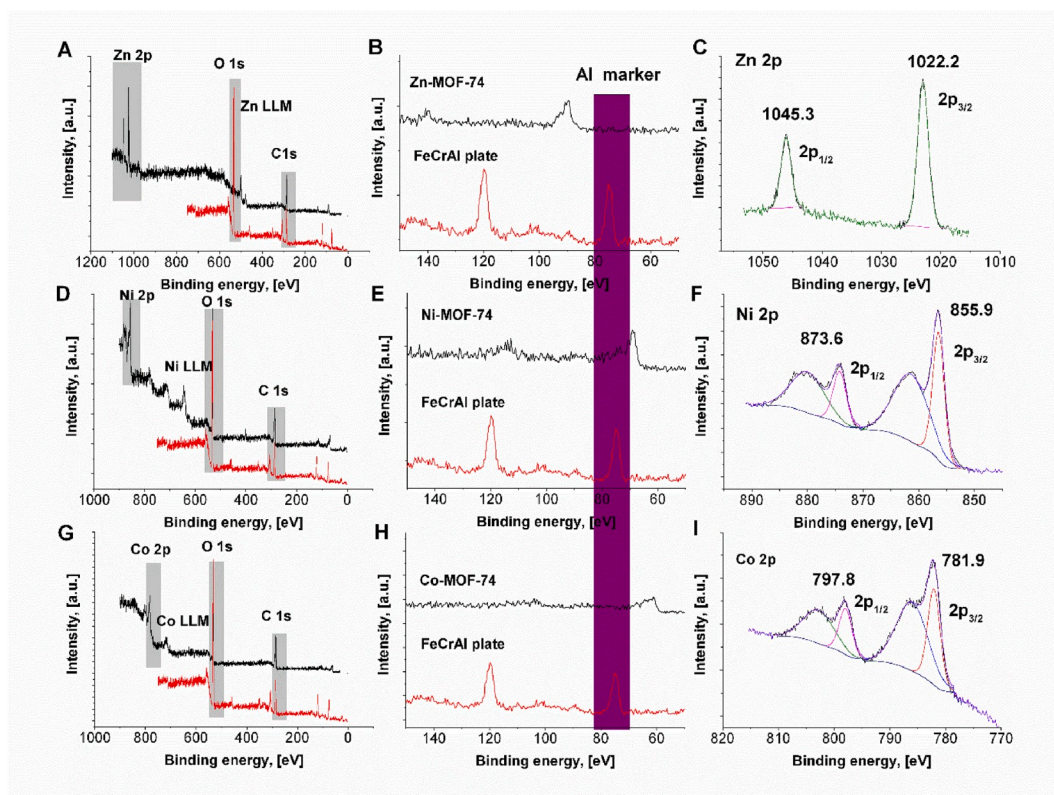
Fig. 2. XPS analysis of prepared of triple deposited M(M = Zn; Ni; Co)-MOF-74 on FeCrAl plates; **Zn- MOF-74 (A–C)**: A) Zn-MOF-74 survey spectrum, B) Al 2p marker region for Zn-MOF-74, C) Zn 2p region for Zn-MOF-74; **Ni-MOF-74 (D–F)**: D) Ni-MOF-74 survey spectrum, E) Al 2p marker region for Ni-MOF-74, F) Ni 2p region for Ni-MOF-74; **Co-MOF-74 (G–I)**: G) Co-MOF-74 survey spectrum, H) Al 2p marker region for Co-MOF-74, I) Co 2p region for Co-MOF-74.
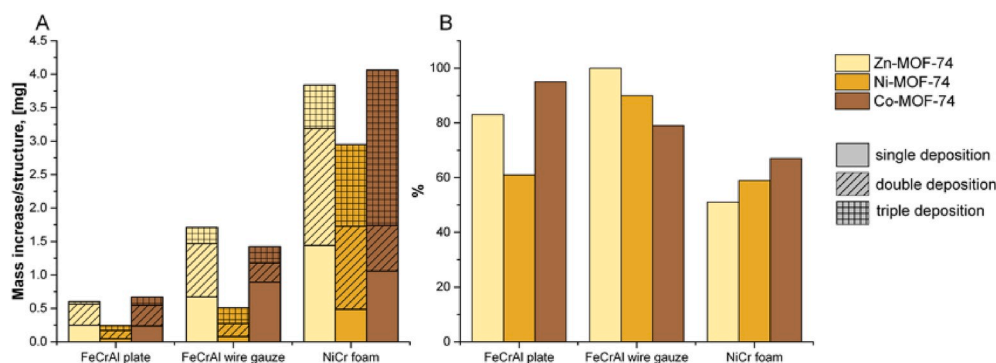

Fig. 3. A) M(M = Zn; Ni; Co)-MOF-74 mass increase/geometrical surface of metallic carrier per deposition; B) Mechanical stability test in ultrasound bath.

deposited on FeCrAl plates. For this support, the individual deposition of Zn- and Co-MOF-74 layers never exceeds 0.32 mg/cm^2 (maximum value achieved for Zn-MOF-74 after double deposition). The maximum mass increase after triple deposition was achieved for Co-MOF-74, and was equal to 0.669 mg/cm^2. The deposition of MOF layers of on FeCrAl wire gauze results in considerable MOF mass increase on metallic support. In general, the MOF loading on wire gauze increases on average by a factor of two, with some minor derogations for Co-MOF-74 at single deposition where this value increases almost four-fold, and for Zn-MOF-74 at triple loading, where the mass increase is almost one order of magnitude higher than for the FeCrAl plate. When considering the total mass increase on the FeCrAl wire gauze in comparison with the FeCrAl plate, the mass loading factor increases in a arrange 2.9-fold for Zn-MOF-74, two-fold for Co-MOF-74 and up to 2.1 times for Ni-MOF-74 (cf. Table S1). The highest metal organic metal loading by *in situ* deposition was achieved for NiCr foam. Analysis of the obtained MOF loading

values (Table S1) reveals that the maximum MOF loading was achieved after triple deposition of Co-MOF-74. Considerable high values were achieved for double deposition of Zn-MOF-74. It must be emphasised that the total mass increase forms the following order Co-MOF-74>Zn-MOF-74>Ni-MOF-74, which is similar to MOF loading on the FeCrAl plate and wire gauze. It must be also pointed out that the Ni-MOF-74 indicated the worst adhesion properties on all considered metallic carriers.

The morphology of deposited coatings on structured supports was determined using two methods: digital photography and SEM microscopy. The results of digital photography imaging are presented in supplementary materials in Figs. S3–S5 for Me (Zn, Ni, Co)-MOF-74 layers deposited on FeCrAl plates, FeCrAl wire gauzes and NiCr foams, respectively. In the case of Zn-MOF-74, the single deposition on each structured support is barely seen in digital pictures. Considerable changes in layer deposition on each structured support may be observed

after double and triple deposition (Figures S3-S5, B and C). For Ni and Co-MOF-74 layers, the single deposition of MOF material may be observed. To determine in detail the morphology of prepared structured catalysts, SEM analysis was performed. To enhance the visibility of SEM images, pseudo colouring by using defined RGB colours determined by UV–Vis spectroscopy was performed. The SEM images are presented in Fig. 4 for three structured carriers, and in Fig. 5 for triple deposited MOF layer on NiCr foams with 2000x magnification. Since the whole matrix contained 27 images per single SEM magnification, the results for each deposition for M(M = Zn; Ni; Co)-MOF-74 are presented in supplementary materials in Figs. S6–S14. The deposition of Zn-MOF-74 on structured carriers is presented in Figs. S6–S8. It can be seen that, after single deposition, surfaces of all three structured carriers at the lowest magnification (200x) do not show any substantial changes in carrier morphology. This changes upon increasing magnification from 2000x up to 5000x. The surface seems to be coated with a thin layer of MOF with visible small crystals of irregular shape. This phenomenon changes after double *in situ* coating (Fig. S7). In this case, even a quick look at the catalyst's surface at low-magnification images reveals the complete coverage of the structured carrier. The crystals began to grow in more regular shape, similar to hexagonal rods. The shape of the Zn-MOF-74 structures is more evident for wire gauze and foam structures. The MOF-74 growth on structures is evident, and good adhesion may be observed. The higher magnifications also reveal smaller crystals found on larger ones (Figure S6-S8 E-F). The triple deposition reveals full surface coverage in all three structured carriers. The MOF crystals reveal

full developed shapes. Detailed analysis of SEM images allows the thickness of the Zn-MOF-74 layers to be determined, which in that case is equal to 40 μm. The important feature of Zn-MOF-74 layers is depicted in Fig. 4 A1, B1, C1 as well as in Figs. S6–S8 G-I, where, for the foam carrier, the MOF crystals are perpendicularly oriented to the foam surface, in contrast to the FeCrAl plates and wire gauzes, where the stochastic orientation prevails.

The SEM images for Ni-MOF-74 are presented in Fig. 4 A2, B2, C2 for triple deposition and in Figs. S9–S11 for single, double and triple deposition. It may be seen that the crystal morphology is far different from that of Zn-MOF-74 crystals. The surfaces of all three structured carriers are covered with spherical crystals with an average diameter of 10 μm. However, it must be emphasised that the crystals form a thin layer which is more visible after double and triple coating of wire gauze and foam carriers. One can observe that surface coverage is uniform after double deposition on structured carriers. After triple deposition, the carriers' surfaces reveal point-crystal growth (Fig. 4 B2 and C2). The thickness of the Ni-MOF-74 layers was equal to the average MOF particle diameter, i.e. 10 μm. The average thickness after triple coating was approx. 30 μm (cf. Fig. S11 G).

The Co-MOF-74 morphology is presented in Fig. 4 A3, B3, C3 and Figs. S12–S14. The crystal morphology exhibits more regular hexagonal shape in comparison with Zn-MOF-74. It can be seen that complete carrier coverage is achieved after single deposition in all considered carriers (Figures S12 A-I). It must be emphasised that, for single deposited Co-MOF-74 on NiCr foam, there is different morphology in
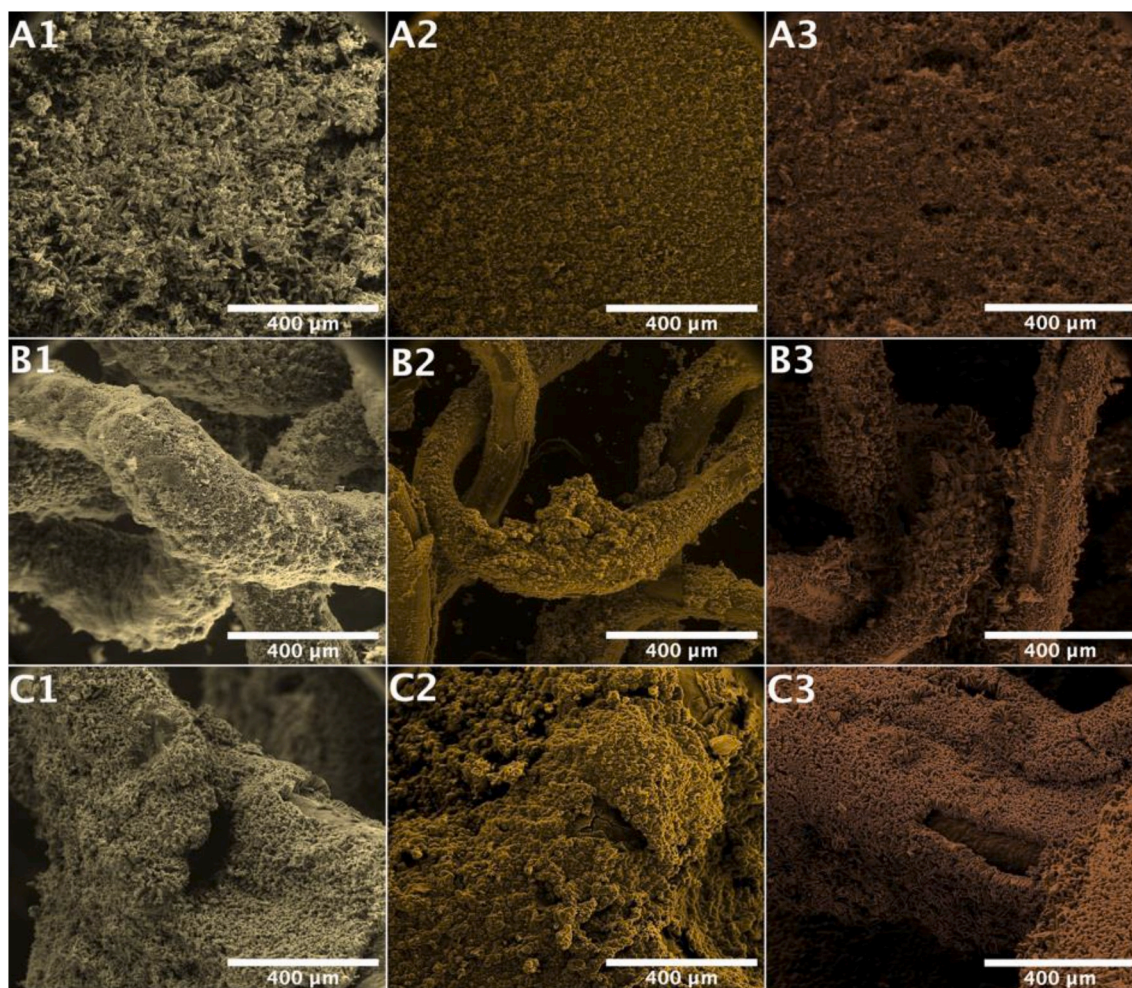

Fig. 4. SEM images of M(M = Zn; Ni; Co)-MOF-74 triple deposited on various metallic supports; A1, B1, C1) Zn-MOF-74, A2, B2, C2) Ni-MOF-74, A3, B3, C3) Co-MOF-74; A) FeCrAl plates, B) FeCrAl wire gauzes, C) NiCr foams.
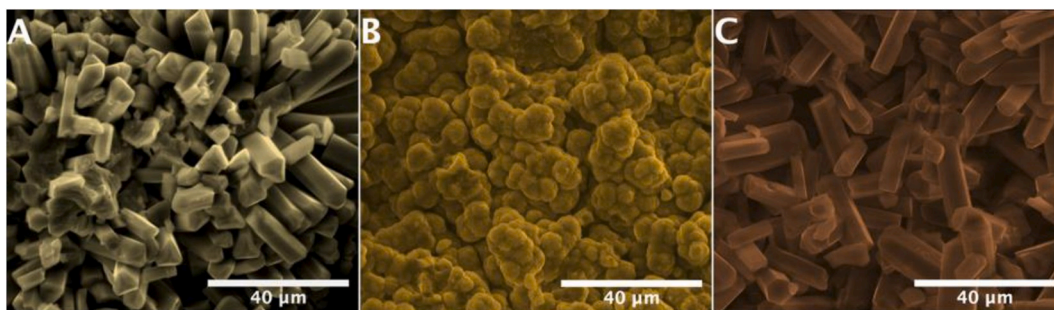
Fig. 5. Magnified (x2k) SEM images of M(M = Zn; Ni; Co)-MOF-74 triple deposited on metallic foam NiCr; A) Zn-MOF-74, B) Ni-MOF-74, C) Co-MOF-74.

comparison with Co-MOF-74 deposited on the FeCrAl plate and wire gauze. The foam surface seems like it was treated by some kind of MOF primer and forms the incubation-like centres for further crystal growth. The morphology of the Co-MOF-74 crystals is similar for all kinds of metal supports after single deposition (Figures S12 A-I). In all considered structured carriers, the hexagonal crystal is perpendicularly oriented to the metallic carriers. The triple deposition of Co-MOF-74, however, causes crystal aggregation, and local crystal spots can be observed especially for the FeCrAl wire gauze and NiCr foam. However, the presence of the local crystal hypertrophies is not evident as in the case of Zn- and Ni-MOF-74 layers. It must also be pointed out that the thickness of the Co-MOF-74 layers is lower than for Ni-MOF-74 and is equal to 20 μm (average single crystal size). Due to the growth of the MOF crystals perpendicular to the support surface, the crystal tends to fill the free space between crystals rather than to overgrow already grown crystals.

The results of the krypton and nitrogen adsorption on bare structured carriers, MOF powders and MOF deposited on metallic supports are summarised in Table 3. The krypton adsorption on structured supports revealed that structured carriers are non-porous solids (Table 3 A). The measured S_{BET} for the FeCrAl plate, wire gauzes and NiCr foams were equal to 0.027, 0.012 and 0.039 m^2/g, respectively. The nitrogen adsorption on powder samples (Table 3 B), collected using the *in situ* solvothermal method, revealed that the specific surface S_{BET} areas of prepared samples were approx. 1000 m^2/g for all prepared powder MOF-74 samples, which corresponds well with the results presented in

the literature [39,42]. Since for the characterisation of metallic structured catalysts with deposited porous metal organic framework layers there is no proposed methodology for the presentation of the S_{BET} results, the data presentation was two-fold. To compare the specific surface of the M(M = Zn; Ni; Co)-MOF-74 layer over representative FeCrAl support, the S_{BET} was referred to the mass of MOF-74 deposited on the metallic carrier. This value was determined gravimetrically after M(M = Zn; Ni; Co)-MOF-74/FeCrAl plate activation. However, to compare the values of the specific surface between the supported catalysts, the S_{BET} was referred to the total mass of the structured catalyst. When analysis of S_{BET} for the FeCrAl plate referred to the deposited MOF layer (Table 3 C), it may be seen that the values for S_{BET} are lower than the calculated specific surface areas for powder samples, and are equal to 331.6 m^2/g for Zn-MOF-74, 823.5 m^2/g for Ni-MOF-74 and 716.7 for m^2/g for Co-MOF-74. It may be observed that a considerable decrease was observed for Zn-MOF-74, where the value of specific surface area was approx. 700 m^2/g lower than for its powder counterpart. The difference between the calculated S_{BET} values may be two-fold. The successful *in situ* synthesis of Zn-MOF-74 over metallic structures was achieved by the optimised triple synthesis, where the primer layer on Zn-MOF-74 was prepared from the zinc acetate solution, whereas double and triple deposition was synthesised by using a nitrate solution as zinc precursor. For Ni- and Co-MOF-74 catalysts, the observed S_{BET} decrease was lower and equal to approx. 200 m^2/g and 300 m^2/g. In this case, however, the Ni- and Co-MOF-74 the triple deposition may cause crystal overgrowth
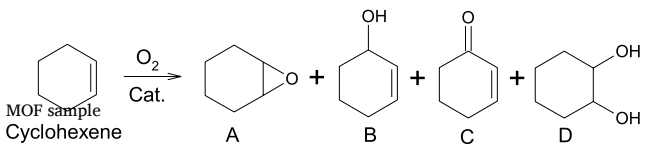
Table 3
Results of the krypton and nitrogen adsorption for prepared samples; A) Kr adsorption results for metallic supports, B) N_2 adsorption measurements for powder M(M = Zn; Ni; Co)-MOF-74 samples, C) N_2 adsorption measurements for triple deposited M(M = Zn; Ni; Co)-MOF-74/FeCrAl referred to deposited MOF mass, D) N_2 adsorption measurements for triple deposited M(M = Zn; Ni; Co)-MOF-74/FeCrAl referred to total mass of structured reactor.

A) Metallic supports		B) Powder samples M(M = Zn; Ni; Co)-MOF-74 powders	
Kr adsorption measurement	S_{BET}, [m^2/g]	N_2 adsorption measurement	S_{BET}, [m^2/g]
FeCrAl plate	0.027	Zn-MOF-74	1023.7
FeCrAl wire gauze	0.012	Ni-MOF-74	1003.3
NiCr foam	0.039	Co-MOF-74	1021.5
C) M(M = Zn; Ni; Co)-MOF-74/FeCrAl (triple deposition) plate referred to deposited MOF mass			
N_2 adsorption measurement	S_{BET}, [m^2/g]		
Zn-MOF-74	331.6		
Ni-MOF-74	823.5		
Co-MOF-74	716.7		
D) Supported M(M = Zn; Ni; Co)-MOF-74 (triple deposition) referred to total structured reactor mass			
N_2 adsorption measurement	Sample	$S_{BET, structured\ reactor}$ [b], [m^2/g]	Calculated mass of deposited MOF, [mg/g $_{structured\ ractor}$]
FeCrAl plate	Zn-MOF-74	0.70	0.80
	Co-MOF-74	26.95	26.40
	Ni-MOF-74	22.60	22.50
FeCrAl wire gauze[a]	Zn-MOF-74	0.40	0.40
	Co-MOF-74	11.30	11.30
	Ni-MOF-74	8.30	9.60
NiCr foam	Zn-MOF-74	0.78	0.80
	Co-MOF-74	65.88	46.9
	Ni-MOF-74	45.80	65.7

[a] Calculated by using eq. (1).
[b] $S_{BET, structured\ reactor}$ related to the total mass of structured reactor.

Table 4
Results of catalytic activity of prepared samples in aerobic oxidation of cyclohexene.

		Pressure	Conversion [%]	Selectivity [%]					Me (Zn, Ni, Co) concentration in post-reaction mixture, mM
				A	B	C	D	other	
blank		atm.	12.0	6.7	62.1	16.9	5.0	9.4	–
blank		10 bar	10.0	6.3	64.0	16.1	4.5	9.1	–
Zn-MOF-74	powder	atm.	66.5	12.5	65.4	13.9	5.8	2.5	0.12
		10 bar	64.8	12.1	58.8	14.0	6.0	9.2	<LOD
	/NiCr foam	10 bar	30.2	9.7	71.9	14.5	1.7	2.2	<LOD
Ni-MOF-74	powder	atm.	59.0	8.7	74.3	13.3	2.3	1.3	<LOD
		10 bar	81.7	8.5	52.7	16.5	7.4	14.9	<LOD
	/NiCr foam	10 bar	34.1	8.3	73.5	14.3	2.5	1.4	<LOD
Co-MOF-74	powder	atm.	52.3	18.9	29.4	22.2	0.0	29.5	2.99
		10 bar	67.9	12.7	35.5	27.7	3.0	21.1	3.03
	/NiCr foam	10 bar	29.1	18.9	30.4	23.3	4.4	23.0	0.39

which may influence the overall S_{BET} value. Additionally, the multiple layer deposition may also influence the availability of micro and mesopores for adsorbed molecule. Analysis of the S_{BET} values referred to the total mass of the structured catalyst (Table 3 D; mass of the metallic carrier + mass of the deposited layer) leads to the general conclusion that the amount of the deposited metallic organic frameworks on the structured support increases in the following order: FeCrAl wire gauze > FeCrAl plate > NiCr foam, which is different than the gravimetrical measurements from Table S1 and Fig. 3. However, it must be emphasised that the values determined by the gravimetrical method were performed after structure catalyst washing after *in situ* deposition and are not impacted by the high temperature UHV activation of catalysts samples in the sorption meter. Analysis of the literature data on TGA analysis of the metal organic frameworks leads to the conclusion that, at approx. 300 °C, M (M = Zn; Ni; Co)-MOF-74 is equal to 30 wt %. of the initial mass [39,40]. In this study, the activation of MOF prior to the N_2 sorption was performed under 250 °C to ensure effective activation. Since the metal supports used in this study are non-porous solids, we can estimate the mass of the catalyst deposited on the surface of the structured supports by formula previously proposed in the literature [50]:

$$m_{MOF\ deposited\ on\ the\ support} = \frac{S_{BET,\ MOF\ deposited\ on\ the\ support}}{S_{BET,\ MOF\ powder}} \cdot m_{MOF\ powder} \cdot 1000,\ [mg]$$

(1)

where: $m_{MOF\ deposited\ on\ the\ support}$ is the approximated mass of the deposited MOF layer on structured support, $S_{BET,\ MOF\ deposited\ on\ the\ support}$ is the specific surface area of the structured reactor (structured support with MOF layer), MOF powder is the mass of the powder used to calculate S_{BET} equal to 1 g. The calculated values of MOF mass deposited on different structured supports lead to the conclusion that the MOF-74 layers are favourably deposited on NiCr foams and FeCrAl plates. However, to fully characterise the effectiveness of the *in situ* layering, the type of the MOF-74 by metal should be considered. It may be seen that the lowest calculated MOF masses were obtained for Zn-MOF-74. Despite the fact that, in the case of Zn-MOF-74, XRD analyses revealed a characteristic pattern for MOF-74 crystals at the metallic support, deep analysis of the SEM pictures for individual depositions shows that the well-defined crystals are formed after triple deposition (Fig. 5 and Figs. S6-S8). The first two layers should therefore be defined as intermediate MOF-layers or primer MOF-layers. The decrease in calculated MOF referred to the total mass of the structured catalysts using N_2 sorption is related to the low contribution of well-crystallised MOF on the overall mass of the deposited layer. The opposite situation can be observed for Ni- and Co-MOF-74 layers deposited on structured carriers.

Here, the total mass of deposited MOF calculated from N_2 sorption gives two-order of magnitude higher values of deposited MOF when comparing to Zn-MOF-74. The SEM results clearly show the growth of well-defined crystals on structured supports after single deposition (Figs. S9-S11).

To determine the molecular nature of the prepared structured MOF catalysts, IR and Raman analyses were performed. The detailed IR analysis of prepared samples using ATR, DRIFT and transmission IR can be found in supporting information (Fig. S15). The characterisation of the active centres in prepared materials was performed by the sorption of two probe molecules: carbon monoxide and CD_3CN. Both probe molecules are commonly used to study acidic and basic properties of heterogeneous catalysts. The results of CO and CD_3CN adsorption are presented in Fig. 6 and Fig. 7, respectively. The low temperature of carbon monoxide adsorption on M(M = Zn; Ni; Co)-MOF-74 gives the rise of the main band at 2160-2180 cm^{-1}, which corresponds to Me^{2+}-CO adducts formed in the prepared metal organic framework catalysts. It has been previously reported in the literature [51,52] that the values of the main CO adsorption bands for M(M = Zn; Ni; Co)-MOF-74 decreases in the following order: Ni (2180 cm^{-1}) > Zn (2173 cm^{-1}) > Co (2162 cm^{-1}). The high C–O stretching frequencies are derivative of the smallest size and the highest polarisation of Ni^{2+} ion for the Ni-MOF-74 sample (Fig. 6 B) [51,52]. It must be emphasised that, upon increase of partial pressure of carbon monoxide, the minor bands at 2150-2100 cm^{-1} and 2200-2250 cm^{-1} can be observed and may be attributed to some combination overtones of ν(CO). It was also observed that, at high CO coverages, for Zn-MOF-74 and Ni-MOF-74 an additional band at around 2135 cm^{-1} is formed, which was previously assigned to liquified CO in the MOF pores [53].

The results of CD_3CN probe molecule adsorption on M(M = Zn; Ni; Co)-MOF-74 catalysts are presented in Fig. 7. The adsorption of CD_3CN probe molecules shows rise of a sharp and intensive band at 2110 cm^{-1}, which is characteristic of deuterated ν(CD_3) vibrations, and two intense bands at 2237 and 2290 cm^{-1}, which may be attributed to physiosorbed CD_3CN and coordinated CN species to Lewis acid sites, respectively [53, 54]. The acidic properties of various MOF materials by using CD_3CN as a probe molecule has recently been reported for MIL-140C (Zr), MIL-140D (Zr) [55], MIL-100 (Al, Fe, Cr) [54]. It must be pointed out that the values of ν(CD_3) and ν(CN) vibrations are similar to those reported for MIL 140C, D and MIL-100 metal organic frameworks, which may lead to the conclusion that they possess similar acid strength.

The complementary experiments of molecular properties of prepared samples were performed by μRaman spectroscopy. The results of μRaman analysis were presented as a μRaman maps (Figs. 8 and 9), for two reasons. The μRaman mapping allowed us to show the distribution
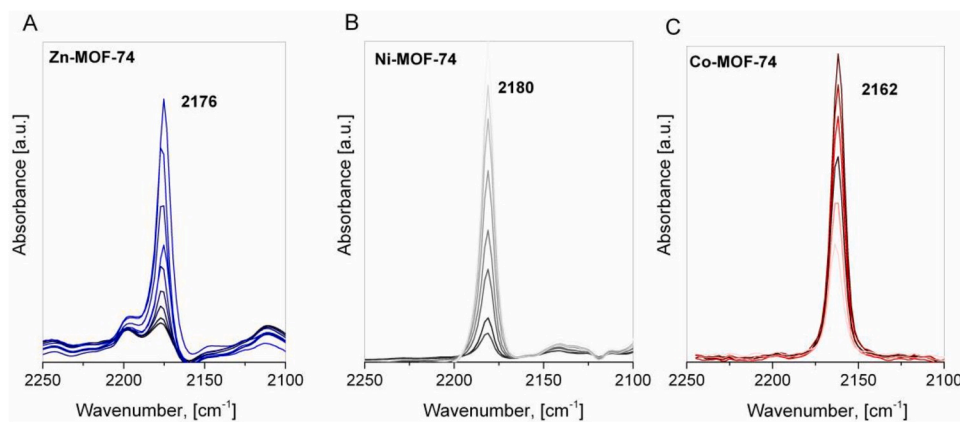
Fig. 6. *In situ* FTIR spectra of CO adsorbed at −100 °C, A) Zn-MOF-74, B) Ni-MOF-74, C) Co-MOF-74.
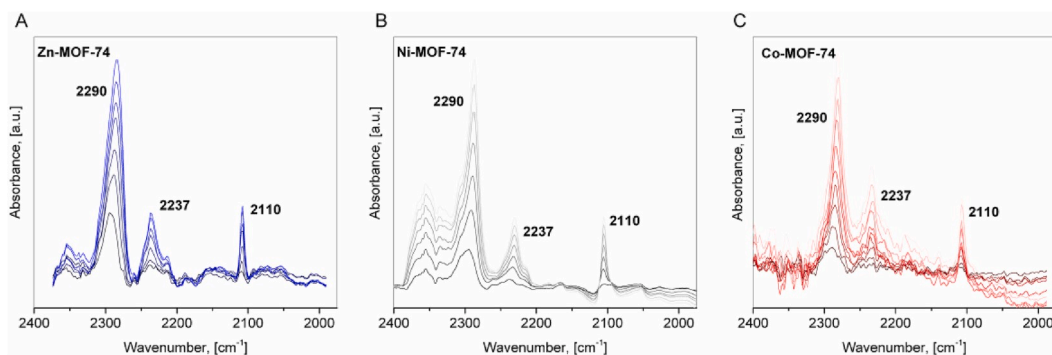

Fig. 7. *In situ* FTIR spectra of CD$_3$CN adsorbed at RT, A) Zn-MOF-74, B) Ni-MOF-74, C) Co-MOF-74.

of the MOF over the metallic carrier. Comparison of the μRaman maps leads to the conclusion that the most uniform distribution was achieved for Ni and Co-MOF-74 samples (Fig. 8 C and D). Indeed, the μRaman maps also exhibit local layer overlapping (brighter spots at μRaman maps), which is in good agreement with SEM images for samples after MOF triple deposition. However, it must also be pointed out that the determination of the surface homogeneity using only μRaman maps must be carried out with a high degree of caution, since μRaman maps for the homogeneous calcined FeCrAl plate also reveal some local increase in Raman intensity. The corresponding Raman spectra (Fig. 9) exhibit the structure of prepared composite samples. The Raman spectrum of the calcined FeCrAl plate (Fig. 9 A) reveals bands at 418, 630 and 750 cm^{-1}, which may be attributed to α-Al$_2$O$_3$ of hexagonal symmetry (band at 418 cm^{-1}) [56], α-Fe$_2$O$_3$ (band 630) and γ-Fe$_2$O$_3$ [57]. The μRaman of the FeCrAl plate may be treated as a marker. Since the depth of the sample penetration is relatively high for Raman scattering, the presence or absence of a marker band may be useful in determining the surface thickness. In our previous work, we reported that the use of various characterisation techniques such as XPS, μRaman and EDX allows the determination of the in-depth distribution of the active phase [58]. Here, we can observe that, for the M(M = Zn; Ni; Co)-MOF-74 composite catalysts deposited on metallic support, there was no signal originating from the metallic support. The Raman spectra of M(M = Zn; Ni; Co)-MOF-74 reveal two main band group regions: to 820 cm^{-1} and 1200-1700 cm^{-1}. The 1200-1700 cm^{-1} reveals bands at 1275, 1412, 1501, 1560 and 1619 cm^{-1}, which may be attributed to ν(C–O) from deprotonated hydroxyls, symmetric ν(COO$^-$) and stretching and deformation vibrations of benzene rings [41], respectively. The bands at lower frequencies, at approx. 820 and 560 cm^{-1}, may originate from benzene ring bending and deformation vibrations, respectively [41,51]. The additional bands, at approx. 413 cm^{-1}, can be due to ν(Me–O) vibrations [51]. Comparison of the Raman maps for M(M = Zn; Ni;

Co)-MOF-74 structured catalysts and the FeCrAl plate lead to the conclusion that the metallic carrier is uniformly covered with the MOF layer. Similar observations can be observed from the analysis of XPS results (cf. Fig. 2 A).

The adherence of the deposited on metallic support M(M = Zn; Ni; Co)-MOF-74 layers was evaluated by using an ultrasound bath mechanical resistance test. This type of examination is frequently used for layer adherence testing in structured catalyst characterisation [37,59, 60]. The results of the MOF layer adherence performance for various structured supports are presented in Fig. 3 B. The results are presented as a percentage of mass loss during ultrasonic irradiation treatment. The best adherence properties were observed for NiCr foams. After the ultrasonic irradiation test for Zn-MOF-74, almost 50% of the deposited material remained at the support surface. This value was slightly lower for the Ni and Co-MOF-74 layer, with 40% and 35% of the material deposited over a metallic foam. The metal organic framework layers deposited on FeCrAl wire gauzes indicated lower adherence to the structured support. In the case of Zn-MOF-74, almost all of the deposited material was removed from the structured support, whereas, for Ni and Co-MOF-74, 10% and 20% of the deposited material remained on the support. Comparison of the layer adherence to the support carrier after mechanical resistance testing for FeCrAl plates and NiCr foams leads to the conclusion that the stability of the deposited MOF material is derivative either of the available geometrical area and its shape or of the total volume of the support which is sonochemically treated. During the mechanical stability experiment, the structures were stochastically placed in an ultrasonic bath. Their natural arrangement in the bath left one of the sides less subjected to ultrasounds. What is more, comparison of the support structure morphology for wire gauzes and foams may lead to the conclusion that intensity of ultrasound waves can be gradually screened by the bone-like structure of NiCr foam. It must be emphasised that the literature reports on the deposition of metal organic frameworks
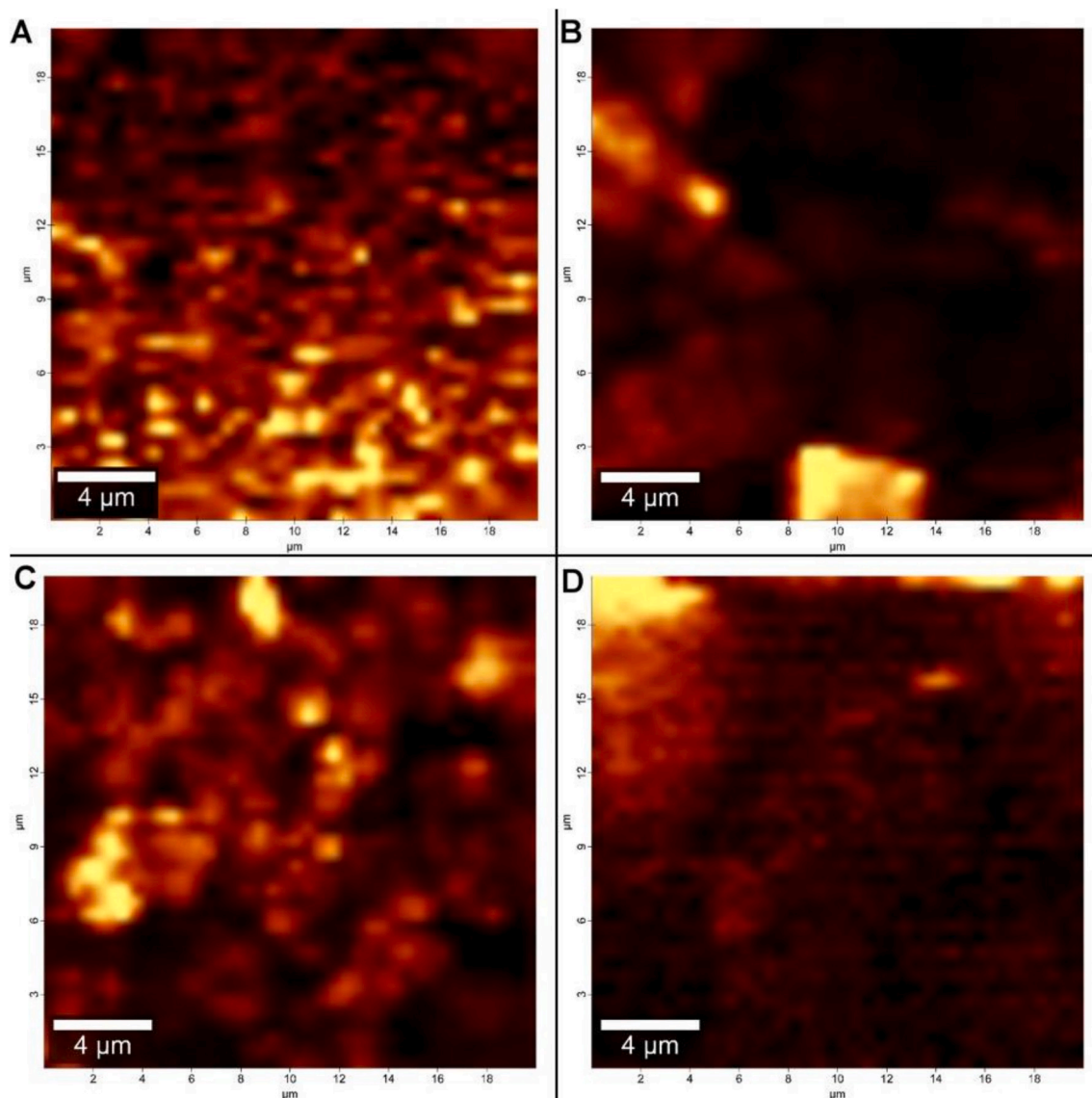
Fig. 8. μRaman maps of M(M = Zn; Ni; Co)-MOF-74 triple deposited on metallic plates, A) calcined metallic plate, B) Zn-MOF-74, C) Ni-MOF-74, D) Co-MOF-74.

on metallic supports is rather scarce, which makes comparison of the obtained results with other literature reports impossible. Since the metal organic frameworks are mainly formed into the desired shapes, such as pellets, foams or monoliths with the addition of a binder [17–19], or as required in the case of their use as the electrodes [13], the influence of the other kinds of forces of the prepared materials has been considered.

The catalytic activity of prepared M(M = Zn; Ni; Co)-MOF-74 powders and Me (Zn, Ni, Co)-MOF-74 deposited on NiCr foams was measured in the aerobic oxidation of cyclohexene. The results are summarised in Table 4. It must be emphasised that bare metallic supports revealed no activity in the aerobic activation oxidation of cyclohexene. The result of catalytic activity is expressed as a function of total conversion of cyclohexene and individual selectivity to the main products: cyclohexene oxide, 2-cyclohexen-1-ol, 2-cyclohexen-1-one and *trans*-cyclohexane-1,2-diol. It may be seen that the activity of all prepared powder catalysts exceeds 50% conversion. The activity of prepared powder samples was: 66.5% for Zn-MOF-74, 59.0% for NiMOF-74 and 52.3% for Co-MOF-74 catalysts. Analysis of the selectivity for prepared samples shows that, for Zn- and Ni-MOF-74 catalysts, the oxidation reaction proceeds mainly to 2-cyclohexen-1-ol and 2-cyclohexen-1-one. In the case of the Zn-MOF-74 catalyst, the selectivity to cyclohexene-1-ol and 2-cyclohexen-1-one was 65.4% and 13.9%,

whereas for Ni-MOF-74 it was 74.3% and 13.3% respectively. The selectivity for the cyclohexane oxide was 12.5 and 8.7% for Zn-MOF-74 and Ni-MOF-74, respectively. However, when analysing the oxidation reaction results for Co-MOF-74, it may be seen that the cobalt oxide favours the epoxidation reaction, with cyclohexane oxide as the main product with almost 19% selectivity, whereas the contributions of the 2-cyclohexen-1-ol, 2-cyclohexen-1-one and the other products were lower. Moreover, among the products, *trans*-cyclohexane-1,2-diol was not detected. Additionally, the contribution of the side products reached 30%. Although in the literature [29,61] we can find some results on cyclohexene catalytic oxidation over Me-MOF-74 catalysts, comparison of the obtained results is impossible due to different synthesis procedures for MOF-based materials and their different physicochemical properties. For example, Ruano e*t al.* [61] synthesised the catalysts from metal acetate solutions (Zn, Co, Ni, Mn and Cu)-MOF-4 with another nanocrystalline structure. Furthermore, the morphology of prepared MOFs in Ref. [61] was far from that of our materials. The S_{BET} values presented in Refs. [61] were 948, 693 and 514 m^2/g for Zn-, Co- and Ni-MOF-74, respectively. These S_{BET} results are considerably lower than the S_{BET} values presented in this work. The next difference between our work and [61] lies in the fact that, during the catalytic activity tests, Ruano et al. [61] used H_2O_2 or *tetr*-buty hydroperoxide (TBHP) as an
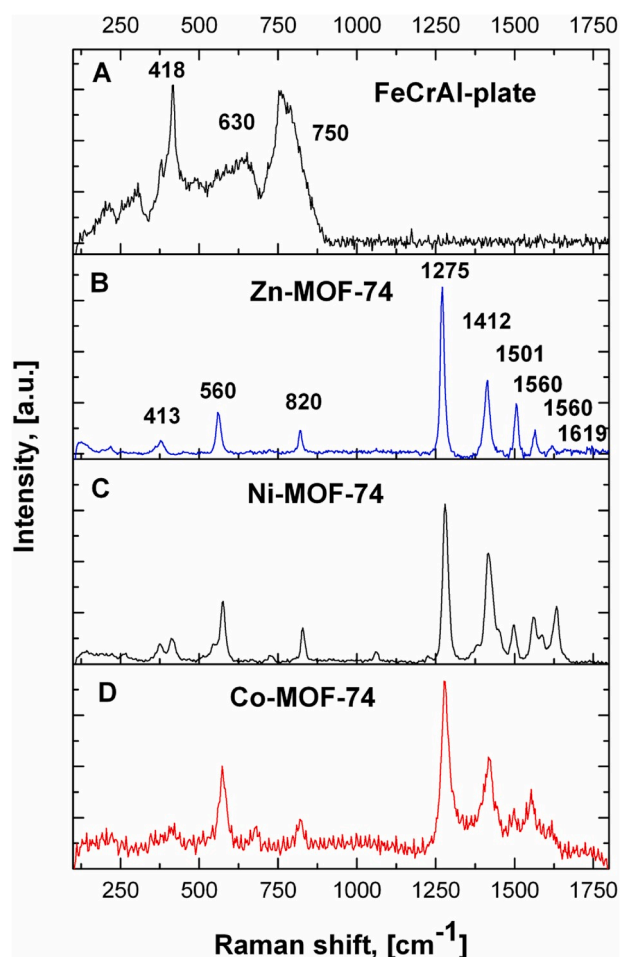
Fig. 9. µRaman spectra to µRaman maps of M(M = Zn; Ni; Co)-MOF-74 triple deposited on FeCrAl metallic plates; A) Zn-MOF-74, B) Ni-MOF-74, C) Co-MOF-74.

oxidising agent together with atmospheric oxygen. Indeed, both oxidising agents can be used to either initialise radical reaction (TBHP) or oxidise cyclohexene, but the oxidising effect is supposed to be higher than in the case of molecular oxygen. Despite this fact, the authors presented cyclohexene conversion reaching 71.5% for Co-MOF-74, 40% for Ni-MOF-74 and 5% for Zn-MOF-74, and analysis of the reaction product was performed by gas chromatography equipped with flame ionisation detector. In relation to the work written by Sun et al. [29], the preparation results were different from the preparation conditions presented in this study.

When analysing the oxidation results under 10 bar O_2 pressure, a general increase of the activity for Ni- and Co-MOF-74 samples can be observed. The conversion of cyclohexene for Ni-MOF-74 increases up to 81.7%, whereas for Co-MOF-74 the conversion is equal to 67.9%. The individual selectivity for the oxidation products changes for Ni-MOF-74 at 10 bar O_2, with considerable increase to 2-cyclohexen-1-one, cyclohexane-1,2-diol and other products. In the case of Co-MOF-74, with the reaction at elevated O_2 pressure, the selectivity of oxidation products remains at the same level, with a slight increase of selectivity to cyclohexane-1,2-diol. For Zn-MOF-74 powder catalysts, we could see no considerable changes in either conversion or selectivity. Catalytic activity was also determined for MOF catalysts deposited *in situ* on NiCr foams. Through analysis of the results of the catalytic activity under 10 bar O_2 pressure over structured M(M = Zn; Ni; Co)-MOF-74 deposited on NiCr foams, a general decrease in conversion of cyclohexene can be observed. It can be seen that, in all considered MOFs deposited on NiCr foams, the conversion of cyclohexene decreased by a factor of two. The

reason of this phenomenon can be explained by the decrease of the effectiveness factor of the catalyst in cyclohexene oxidation. Despite the fact that in all catalytic experiments the same catalyst amount was used (50.0 mg), it must be pointed out that, in the case of powder catalysts, the availability of the active sites is higher due to the wide distribution of catalysts in the reacting mixture. The comparison of the SEM results in Figs. S6-S14 for both supported catalysts and powder MOF-based materials shows that the size of the individual grains varies from 5 to 10 µm, whereas the thickness of the deposited layer is as high as 40 µm. The considerable thickness of the MOF layer on the support may lead to a considerable decrease in the catalytic activity of prepared materials according to the Thiele modulus. However, the calculation of the Thiele modulus and effectiveness factor calculations exceeds the scope of this article, indicating future directions for the application of structured reactors with deposited MOFs.

The characterisation of MOF materials in the catalytic oxidation of cyclohexene should consider also a factor related with the migration of a metal from MOF structure to the reaction solution. The results of the metal content in post-reaction mixtures are presented in Table 4. Analysis of the obtained results leads to the conclusion that, in the case of Zn-MOF-74 and Ni-MOF-74, the metal content in the post-reaction mixture was below the detection limit. Only small amounts of zinc ions were detected in the post-reaction mixture (0.12 mM). Noticeable amounts of metal in the post-reaction mixture were observed for Co-MOF-74. The amount to detected cobalt was approx. 3 mmol for the Co-MOF-74 powder sample for the oxidation reaction under atmospheric and 10 bar O_2 pressure. However, for MOF deposited on NiCr, the value of detected Co was one order of magnitude lower, and was equal to 0.39. The decrease of cobalt migration to the reaction mixture may be related with the generally lower activity of the Co-MOF-74/NiCr catalyst and the good adhesion of the MOF to the NiCr foam surface. It must be emphasised that, in the case of MOF catalysts deposited on NiCr foams, the catalysts were placed in the reaction vessel and simply removed after the reaction, whereas cobalt catalysts in powder form required additional filtration to separate the reacting mixture and powder catalyst. The lack of additional filtration of the post-reaction mixture and catalyst in the case of MOF deposited on NiCr may be a fundamental step towards the wider application of MOF materials as heterogeneous catalysts.

4. Conclusions

The aim of this paper was to obtain and characterise thin metal organic framework layers on various metallic structured supports by using spectroscopic and microscopic methods, and to determine their potential application in the catalytic oxidation of cyclohexene. The *in situ* deposition of metallic organic framework thin layers consists of three steps, including support pre-treatment, *in situ* solvothermal deposition and MOF-layer activation to remove residual solvents from synthesis protocol. The prepared structured carriers with deposited MOF-74 layers were characterised with various characterisation techniques to determine the surface morphology and their molecular structure. The *in situ* deposition of metal organic frameworks was the most effective for Zn- and Co-MOF-74 on NiCr foams, giving the approx. 4 mg/cm^2 mass increase after triple coating. We have indicated that there is no difference in molecular structure between *in situ* deposited and non-deposited crystalline phase of metal organic frameworks. The high mechanical resistance of prepared M(M = Zn; Ni; Co)-MOF-74 layers on NiCr foams and FeCrAl plates was confirmed by the ultrasonic irradiation performance.

The activity of prepared MOF catalysts both in powder form and MOF deposited on NiCr foams was measured in the catalytic oxidation of cyclohexene. The prepared catalysts revealed high activity in the studied reaction, with the conversion exceeding 50% for powder catalysts under both atmospheric and elevated pressures. The catalysts deposited on NiCr foams revealed twice lower conversion in comparison with their

powder counterparts. However, the use of structured catalysts did not require their additional filtration from the reaction mixture, which makes them favourable for further testing as heterogeneous catalysts in the organic reagents oxidation.

We believe that the *in situ* deposition of metal organic frameworks from Me₂(dobdc) group, proposed in this study, will lead to the substantial development of MOF materials and their further application in heterogeneous catalysis as structured reactors.

Declaration of competing interest

The authors declare that they have no known competing financial interests or personal relationships that could have appeared to influence the work reported in this paper.

CRediT authorship contribution statement

P.J. Jodłowski: Formal analysis, Investigation, Data curation, Writing - review & editing. **G. Kurowski:** Formal analysis, Investigation. **K. Dymek:** Formal analysis, Investigation. **R.J. Jędrzejczyk:** Formal analysis, Investigation. **P. Jeleń:** Formal analysis, Investigation. **Ł. Kuterasiński:** Formal analysis, Investigation. **A. Gancarczyk:** Formal analysis, Investigation. **A. Węgrzynowicz:** Formal analysis, Investigation. **T. Sawoszczuk:** Formal analysis, Investigation. **M. Sitarz:** Formal analysis.

Acknowledgments

Appendix A. Supplementary data

Supplementary data to this article can be found online at https://doi.org/10.1016/j.micromeso.2020.110249.

References

[1] S.R. Batten, N.R. Champness, X.-M. Chen, J. Garcia-Martinez, S. Kitagawa, L. Öhrström, et al., Terminology of metal–organic frameworks and coordination polymers (IUPAC Recommendations 2013), Pure Appl. Chem. 85 (2013) 1715–1724, https://doi.org/10.1351/PAC-REC-12-11-20.

[2] N. Stock, S. Biswas, Synthesis of metal-organic frameworks (MOFs): routes to various MOF topologies, morphologies, and composites, Chem. Rev. 112 (2012) 933–969, https://doi.org/10.1021/cr200304e.

[3] Y. Mao, J. Li, W. Cao, Y. Ying, P. Hu, Y. Liu, et al., General incorporation of diverse components inside metal-organic framework thin films at room temperature, Nat. Commun. 5 (2014) 1–9, https://doi.org/10.1038/ncomms6532.

[4] V.V. Butova, M.A. Soldatov, A.A. Guda, K.A. Lomachenko, C. Lamberti, Metal-organic frameworks: structure, properties, methods of synthesis and characterization, Russ. Chem. Rev. 85 (2016) 280–307, https://doi.org/10.1070/RCR4554.

[5] J. Liu, P.K. Thallapally, B.P. McGrail, D.R. Brown, J. Liu, Progress in adsorption-based CO₂ capture by metal–organic frameworks, Chem. Soc. Rev. 41 (2012) 2308–2322, https://doi.org/10.1039/C1CS15221A.

[6] H. Furukawa, K.E. Cordova, M. O'Keeffe, O.M. Yaghi, The Chemistry and applications of metal-organic frameworks, Science (2013) 341, 80-, http://science.sciencemag.org/content/341/6149/1230444.abstract.

[7] G. Zhu, R. Graver, L. Emdadi, B. Liu, K.Y. Choi, D. Liu, Synthesis of zeolite@metal-organic framework core-shell particles as bifunctional catalysts, RSC Adv. 4 (2014) 30673–30676, https://doi.org/10.1039/c4ra03129f.

[8] R. Krishna, Methodologies for evaluation of metal-organic frameworks in separation applications, RSC Adv. 5 (2015) 52269–52295, https://doi.org/10.1039/c5ra07830j.

[9] R. Krishna, Methodologies for evaluation of metal-organic frameworks in separation applications, RSC Adv. 5 (2015) 52269–52295, https://doi.org/10.1039/c5ra07830j.

[10] K. Leus, Y. Liu, P. Van Der Voort, Metal-Organic Frameworks as selective or chiral oxidation catalysts, Catal. Rev. - Sci. Eng. 56 (2017) 1–56, https://doi.org/10.1080/01614940.2014.864145.

[11] R.M. Heck, S. Gulati, R.J. Farrauto, The application of monoliths for gas phase catalytic reactions, Chem. Eng. J. 82 (2001) 149–156, https://doi.org/10.1016/S1385-8947(00)00365-X.

[12] Z.G. Gu, J. Zhang, Epitaxial growth and applications of oriented metal–organic framework thin films, Coord. Chem. Rev. 378 (2019) 513–532, https://doi.org/10.1016/j.ccr.2017.09.028.

[13] Z. Jiang, T. Liu, L. Yan, J. Liu, F. Dong, M. Ling, et al., Metal-organic framework nanosheets-guided uniform lithium deposition for metallic lithium batteries, Energy Storage Mater. 11 (2018) 267–273, https://doi.org/10.1016/j.ensm.2017.11.003.

[14] X. Ma, Y. Chai, P. Li, B. Wang, Metal-organic framework films and their potential applications in environmental pollution control, Acc. Chem. Res. 52 (2019) 1461–1470, https://doi.org/10.1021/acs.accounts.9b00113.

[15] A. Knebel, P. Wulfert-Holzmann, S. Friebe, J. Pavel, I. Strauß, A. Mundstock, et al., Hierarchical nanostructures of metal-organic frameworks applied in gas separating ZIF-8-on-ZIF-67 membranes, Chem. Eur J. 24 (2018) 5728–5733, https://doi.org/10.1002/chem.201705562.

[16] J.L. Zhuang, D. Ar, X.J. Yu, J.X. Liu, A. Terfort, Patterned deposition of metal-organic frameworks onto plastic, paper, and textile substrates by inkjet printing of a precursor solution, Adv. Mater. 25 (2013) 4631–4635, https://doi.org/10.1002/adma.201301626.

[17] B. Valizadeh, T.N. Nguyen, K.C. Stylianou, Shape engineering of metal–organic frameworks, Polyhedron 145 (2018) 1–15, https://doi.org/10.1016/j.poly.2018.01.004.

[18] Y. Chen, X. Huang, S. Zhang, S. Li, S. Cao, X. Pei, et al., Shaping of metal-organic frameworks: from fluid to shaped bodies and robust foams, J. Am. Chem. Soc. 138 (2016) 10810–10813, https://doi.org/10.1021/jacs.6b06959.

[19] A. Garai, W. Shepherd, J. Huo, D. Bradshaw, Biomineral-inspired growth of metal-organic frameworks in gelatin hydrogel matrices, J. Mater. Chem. B. 1 (2013) 3678–3684, https://doi.org/10.1039/c3tb20814a.

[20] X. Wang, H. Xue, Z. Na, D. Yin, Q. Li, C. Wang, et al., Metal organic frameworks route to prepare two-dimensional porous zinc-cobalt oxide plates as anode materials for lithium-ion batteries, J. Power Sources 396 (2018) 659–666, https://doi.org/10.1016/j.jpowsour.2018.06.086.

[21] N.V. Maksimchuk, K.A. Kovalenko, V.P. Fedin, O.A. Kholdeeva, Cyclohexane selective oxidation over metal-organic frameworks of MIL-101 family: superior catalytic activity and selectivity, Chem. Commun. 48 (2012) 6812–6814, https://doi.org/10.1039/c2cc31877f.

[22] I.M. Denekamp, M. Antens, T.K. Slot, G. Rothenberg, Selective catalytic oxidation of cyclohexene with molecular oxygen: radical versus nonradical pathways, ChemCatChem 10 (2018) 1035–1041, https://doi.org/10.1002/cctc.201701538.

[23] Y. Cao, H. Yu, F. Peng, H. Wang, Selective allylic oxidation of cyclohexene catalyzed by nitrogen-doped carbon nanotubes, ACS Catal. 4 (2014) 1617–1625, https://doi.org/10.1021/cs500187q.

[24] M. Kohantorabi, M.R. Gholami, Cyclohexene oxidation catalyzed by flower-like core-shell Fe3O4@Au/metal organic frameworks nanocomposite, Mater. Chem. Phys. 213 (2018) 472–481, https://doi.org/10.1016/j.matchemphys.2018.04.051.

[25] A.L. Koritzke, J.C. Davis, R.L. Caravan, M.G. Christianson, D.L. Osborn, C. A. Taatjes, et al., QOOH-mediated reactions in cyclohexene oxidation, Proc. Combust. Inst. 37 (2019) 323–335, https://doi.org/10.1016/j.proci.2018.05.029.

[26] Y. Xue, W. Sun, Q. Wang, L. Cao, J. Yang, Sparsely loaded Pt/MIL-96(Al) MOFs catalyst with enhanced activity for H2-SCR in a gas diffusion reactor under 80 °C, Chem. Eng. J. 335 (2018) 612–620, https://doi.org/10.1016/j.cej.2017.11.011.

[27] A. Cybulski, J.A. Moulijn, Structured Catalysts and Reactors, CRC Press, 2005. https://books.google.pl/books?id=r56LOldJ_N4C.

[28] V.K. Ambili, Studies on Catalysis by Ordered Mesoporous SBA-15 Materials Modified with Transition Metals, Cochin University of Science and Technology, 2011.

[29] D. Sun, F. Sun, X. Deng, Z. Li, Mixed-metal strategy on metal-organic frameworks (MOFs) for functionalities expansion: Co substitution induces aerobic oxidation of cyclohexene over inactive Ni-MOF-74, Inorg. Chem. 54 (2015) 8639–8643, https://doi.org/10.1021/acs.inorgchem.5b01278.

[30] L. Giani, C. Cristiani, G. Groppi, E. Tronconi, Washcoating method for Pd/γ-Al2O3 deposition on metallic foams, Appl. Catal. B Environ. 62 (2006) 121–131, https://doi.org/10.1016/j.apcatb.2005.07.003.

[31] J. Campbell, B. Tokay, Controlling the size and shape of Mg-MOF-74 crystals to optimise film synthesis on alumina substrates, Microporous Mesoporous Mater. 251 (2017) 190–199, https://doi.org/10.1016/j.micromeso.2017.05.058.

[32] J.L.C. Rowsell, O.M. Yaghi, Effects of functionalization, catenation, and variation of the metal oxide and organic linking units on the low-pressure hydrogen adsorption properties of metal-organic frameworks, J. Am. Chem. Soc. 128 (2006) 1304–1315, https://doi.org/10.1021/ja056639q.

[33] J. Ma, A.P. Kalenak, A.G. Wong-Foy, A.J. Matzger, Rapid guest exchange and ultra-low surface tension solvents optimize metal–organic framework activation, Angew. Chem. Int. Ed. 56 (2017) 14618–14621, https://doi.org/10.1002/anie.201709187.

[34] F. Yin, S. Ji, B. Chen, Z. Zhou, H. Liu, C. Li, Catalytic combustion of methane over Ce 1 À x La x O 2 À x/2/Al 2 O 3/FeCrAl catalysts 310 (2006) 164–173, https://doi.org/10.1016/j.apcata.2006.05.034.

[35] S. Zhao, J. Zhang, D. Weng, X. Wu, A method to form well-adhered g -Al 2 O 3 layers on FeCrAl metallic supports 167 (2003) 97–105, https://doi.org/10.1016/S0257-8972(02)00859-9.

[36] X. Wu, D. Weng, S. Zhao, W. Chen, Influence of an aluminized intermediate layer on the adhesion of a g -Al 2 O 3 washcoat on, FeCrAl 190 (2005) 434–439, https://doi.org/10.1016/j.surfcoat.2004.03.007.

[37] P.J. Jodłowski, D.K. Chlebda, R.J. Jędrzejczyk, A. Dziedzicka, Ł. Kuterasiński, M. Sitarz, Characterisation of well-adhered ZrO2 layers produced on structured reactors using the sonochemical sol–gel method, Appl. Surf. Sci. 427 (2018) 563–574, https://doi.org/10.1016/j.apsusc.2017.08.057.

[38] M. Valentini, G. Groppi, C. Cristiani, M. Levi, E. Tronconi, P. Forzatti, The deposition of γ-Al2O3layers on ceramic and metallic supports for the preparation of structured catalysts, Catal. Today 69 (2001) 307–314, https://doi.org/10.1016/S0920-5861(01)00383-2.

[39] A.K. Das, R.S. Vemuri, I. Kutnyakov, B.P. McGrail, R.K. Motkuri, An efficient synthesis strategy for metal-organic frameworks: dry-gel synthesis of MOF-74 framework with high yield and improved performance, Sci. Rep. 6 (2016) 1–7, https://doi.org/10.1038/srep28050.

[40] R. Zhang, C.-A. Tao, R. Chen, L. Wu, X. Zou, J. Wang, Ultrafast synthesis of Ni-MOF in one minute by ball milling, Nanomaterials 8 (2018) 1067, https://doi.org/10.3390/nano8121067.

[41] F. Bonino, S. Chavan, J.G. Vitillo, E. Groppo, G. Agostini, C. Lamberti, et al., Local structure of CPO-27-Ni metallorganic framework upon dehydration and coordination of NO, Chem. Mater. 20 (2008) 4957–4968, https://doi.org/10.1021/cm800686k.

[42] L. Garzon-Tovar, A. Sarne-Sanchez, C. Carbonell, I. Imaz, D. Maspoch, Optimised room temperature, water-based synthesis of CPO-27- M metal-organic frameworks with high space-time yields, J. Mater. Chem. A. 3 (2015) 20819–20826, https://doi.org/10.1039/x0xx00000x.

[43] S.D. Ponja, I.P. Parkin, C.J. Carmalt, Synthesis and material characterization of amorphous and crystalline (α-) Al2O3: via aerosol assisted chemical vapour deposition, RSC Adv. 6 (2016) 102956–102960, https://doi.org/10.1039/c6ra24018f.

[44] J. Łojewska, A. Knapik, A. Kołodziej, P. Jodłowski, Far field combined AFM and micro-Raman imaging for characterisation of surface of structured catalysts: example of Pd doped CoOx catalysts on precalcined kanthal steel, Top. Catal. 56 (2013) 1088–1095, https://doi.org/10.1007/s11244-013-0074-6.

[45] V. Demange, J.W. Anderegg, J. Ghanbaja, F. Machizaud, D.J. Sordelet, M. Besser, et al., Surface oxidation of Al-Cr-Fe alloys characterized by X-ray photoelectron spectroscopy, Appl. Surf. Sci. 173 (2001) 327–338, https://doi.org/10.1016/S0169-4332(01)00011-3.

[46] Z. Zhang, Y. Xiao, M. Cui, J. Tang, Z. Fei, Q. Liu, et al., Modulating the basicity of Zn-MOF-74 via cation exchange with calcium ions, Dalton Trans. 48 (2019) 14971–14974, https://doi.org/10.1039/c9dt03332g.

[47] M. Mukoyoshi, H. Kobayashi, K. Kusada, M. Hayashi, T. Yamada, M. Maesato, et al., Hybrid materials of Ni NP@MOF prepared by a simple synthetic method, Chem. Commun. 51 (2015) 12463–12466, https://doi.org/10.1039/c5cc04663g.

[48] C. Huang, R. Liu, W. Yang, Y. Li, J. Huang, H. Zhu, Enhanced catalytic activity of MnCo-MOF-74 for highly selective aerobic oxidation of substituted toluene, Inorg. Chem. Front. 5 (2018) 1923–1932, https://doi.org/10.1039/c8qi00429c.

[49] I. Nova, A. Beretta, G. Groppi, L. Lietti, E. Tronconi, P. Forzatti, Monolithic catalysts for NOx removal from stationary sources, in: A. Cybulski, J.A. Moulijn (Eds.), Struct. Catal. React, CRC Press, 2005, pp. 171–214.

[50] E. Hędrzak, A. Węgrzynowicz, R. Rachwalik, B. Sulikowski, P. Michorczyk, Monoliths with MFI zeolite layers prepared with the assistance of 3D printing: characterization and performance in the gas phase isomerization of A-pinene, Appl. Catal. A Gen. 579 (2019) 75–85, https://doi.org/10.1016/j.apcata.2019.04.017.

[51] S. Chavan, F. Bonino, J.G. Vitillo, E. Groppo, C. Lamberti, P.D.C. Dietzel, et al., Response of CPO-27-Ni towards CO, N2 and C2H 4, Phys. Chem. Chem. Phys. 11 (2009) 9811–9822, https://doi.org/10.1039/b907258f.

[52] S. Chavan, J.G. Vitillo, E. Groppo, F. Bonino, C. Lamberti, P.D.C. Dietzel, et al., CO Adsorption on CPO-27-Ni Coordination Polymer : Spectroscopic Features and Interaction Energy, (2009) 3292-3299.

[53] S. Bordiga, E. Escalona Platero, C. Otero Areán, C. Lamberti, A. Zecchina, Low temperature CO adsorption on Na-ZSM-5 zeolites: an FTIR investigation, J. Catal. 137 (1992) 179–185, https://doi.org/10.1016/0021-9517(92)90147-A.

[54] C. Volkringer, H. Leclerc, J.C. Lavalley, T. Loiseau, G. Férey, M. Daturi, et al., Infrared spectroscopy investigation of the acid sites in the metal-organic framework aluminum trimesate MIL-100(Al), J. Phys. Chem. C 116 (2012) 5710–5719, https://doi.org/10.1021/jp210671t.

[55] F. Bonino, C. Lamberti, S. Bordiga, IR and Raman spectroscopies probing MOFs structure, defectivity, and reactivity, Chem. Met. Fram. Synth. Charact. Appl. (2016) 657–690, https://doi.org/10.1002/9783527693078.ch22.

[56] J. Łojewska, A. Knapik, P. Jodłowski, T. Łojewski, A. Kołodziej, Topography and morphology of multicomponent catalytic materials based on Co, Ce and Pd oxides deposited on metallic structured carriers studied by AFM/Raman interlaced microscopes, Catal. Today 216 (2013) 11–17, https://doi.org/10.1016/j.cattod.2013.05.008.

[57] R. Otero-Lorenzo, M.C. Weber, P.A. Thomas, J. Kreisel, V. Salgueiriño, Interplay of chemical structure and magnetic order coupling at the interface between Cr2O3 and Fe3O4 in hybrid nanocomposites, Phys. Chem. Chem. Phys. 16 (2014) 22337–22342, https://doi.org/10.1039/c4cp01898b.

[58] P.J. Jodłowski, R.J. Jędrzejczyk, A. Rogulska, A. Wach, P. Kuśtrowski, M. Sitarz, et al., Spectroscopic characterization of Co3O4 catalyst doped with CeO2 and PdO for methane catalytic combustion, Spectrochim. Acta - Part A Mol. Biomol. Spectrosc. 131 (2014) 696–701, https://doi.org/10.1016/j.saa.2014.05.027.

[59] V. Meille, S. Pallier, G.V. Santa Cruz Bustamante, M. Roumanie, J.P. Reymond, Deposition of γ-Al2O3layers on structured supports for the design of new catalytic reactors, Appl. Catal. A Gen. 286 (2005) 232–238, https://doi.org/10.1016/j.apcata.2005.03.028.

[60] V. Meille, Review on methods to deposit catalysts on structured surfaces, Appl. Catal. A Gen. 315 (2006) 1–17, https://doi.org/10.1016/j.apcata.2006.08.031.

[61] D. Ruano, M. Díaz-García, A. Alfayate, M. Sánchez-Sánchez, Nanocrystalline M-MOF-74 as heterogeneous catalysts in the oxidation of cyclohexene: correlation of the activity and redox potential, ChemCatChem 7 (2015) 674–681, https://doi.org/10.1002/cctc.201402927.